Global and Planetary Change 128 (2015) 61–71

Contents lists available at ScienceDirect

Global and Planetary Change

journal homepage: www.elsevier.com/locate/gloplacha

Accelerated mass loss from Greenland ice sheet: Links to atmospheric circulation in the North Atlantic

Ki-Weon Seo [a,*], Duane E. Waliser [b], Choon-Ki Lee [c], Baijun Tian [b], Ted Scambos [d], Baek-Min Kim [c], Jan H. van Angelen [e], Michiel R. van den Broeke [e]

[a] Department of Earth Science Education, Seoul National University, Seoul 151-742, Republic of Korea
[b] Jet Propulsion Laboratory, California Institute of Technology, Pasadena, CA 91109-8099, USA
[c] Korea Polar Research Institute, Incheon 406-840, Republic of Korea
[d] National Snow and Ice Data Center, University of Colorado Boulder, Boulder, CO 80309, USA
[e] Institute for Marine and Atmospheric Research, Utrecht University, 3584 CC Utrecht, The Netherlands

ARTICLE INFO

Article history:
Received 5 October 2013
Received in revised form 12 February 2015
Accepted 13 February 2015
Available online 23 February 2015

Keywords:
Greenland ice mass loss acceleration
Surface mass balance
North Atlantic oscillation

ABSTRACT

Understanding the mechanisms that drive the mass imbalance of the Greenland ice sheet (GrIS) is critical to the accurate projection of its contribution to future sea level rise. Greenland's ice mass loss has been accelerating recently. Using satellite Earth-gravity and regional climate model data, we show that the acceleration rate of Greenland ice mass loss from 2003 to 2012 is -13.9 ± 2.0 Gt/yr^2, which results mainly from an increase of meltwater runoff (-6.3 ± 1.1 Gt/yr^2) and a decrease of precipitation (-4.8 ± 1.1 Gt/yr^2). Before the extreme surface melting in the summers of 2010 and 2012, the decrease of precipitation (-9.7 ± 2.5 Gt/yr^2) was a larger contributor to the ice mass loss acceleration than the increase of runoff (-2.1 ± 2.2 Gt/yr^2). Furthermore, we show that the North Atlantic Oscillation (NAO) is linked to the precipitation decrease during summer, and its recent influence to Greenland is anomalously large possibly due to the change in atmospheric circulation in the North Atlantic. These results indicate that inter-annual climate variability is playing a significant role in the recently observed Greenland ice mass loss acceleration, underscoring the difficulty of projecting future sea level rise based on the recent observations of GrIS mass loss.

1. Introduction

Greenland ice sheet (GrIS) stores enough freshwater to cause about 7 m average global eustatic sea level rise if it were to melt completely (Dowdeswell, 2006). For the past two decades, from 1992 to 2012, Greenland's net ice mass flux to the oceans has averaged about −142 Gt/yr (equivalent to a 0.39 mm/yr rise in global sea level) while the net ice mass flux to the oceans from Antarctica is about −71 Gt/yr, only half of that over Greenland (Shepherd et al., 2012). Therefore, GrIS is one of the most important contributors to the current sea level rise.

Numerous studies based on satellite remote sensing and regional climate modeling (Luthcke et al., 2006; Rignot and Kanagaratnam, 2006; Rignot et al., 2011) have suggested that GrIS mass loss has accelerated over the past 20 yr (-21.9 ± 1 Gt/yr^2 in 1992–2009). In particular, during the last decade, GRACE gravimetry data has shown a clear acceleration (-30 ± 11 Gt/yr^2 in 2002–2009) of GrIS mass loss (Velicogna, 2009), and the altimetry data have shown a distinct dynamic thinning (−0.84 m/yr in 2003–2009) (Pritchard et al., 2009), mainly a result of accelerated ice flow in faster flowing glaciers (100 m/yr and higher). The accelerated ice mass loss might result from one or more factors: increased ice discharge, increased run-off due to melt, or a decrease of mass gained by precipitation.

Any long-term acceleration of GrIS ice mass loss will have a significant impact on future sea level rise forecasts (Wouters et al., 2013). In order to more accurately project future sea level rise contributions from Greenland's ice mass loss, it is important to accurately attribute the contribution of mass loss and gain components to the total mass variation. Van den Broeke et al. (2009) separated those components based on remote sensing observations and a regional climate model, and showed that the decrease of surface mass balance (decrease of precipitation and increase of runoff) and increase of ice discharge contributed about equally to the GrIS ice mass loss from 2000 to 2008. Sasgen et al. (2012) showed that ice mass loss acceleration in the east, south-east and south-west of Greenland can be partly attributed to the inter-annual variations of precipitation. More recently, Wouters et al. (2013) showed that the observed acceleration of GrIS mass loss over the relatively short GRACE epoch is not significantly larger than that caused by the stochastic climate variability in GrIS.

These results indicate that the acceleration of GrIS mass loss is at least partly due to variation of 'meltwater runoff and precipitation.

* Corresponding author.
E-mail address: seokiweon@snu.ac.kr (K.-W. Seo).

http://dx.doi.org/10.1016/j.gloplacha.2015.02.006
0921-8181/

In addition, the North Atlantic Oscillation (NAO) is known to be highly correlated with Greenland precipitation rate (Appenzeller et al., 1998; Mosley-Thompson et al., 2005; Box, 2006). Satellite altimeter (ERS-1/2) data over Greenland revealed that variations in height of the Greenland ice sheet are correlated with the NAO (Johannessen et al., 2005). Therefore, it is possible that the precipitation decrease driven by the NAO results in a considerable contribution to the acceleration of GrIS mass loss. In this study, we examine the ice mass loss acceleration observed by GRACE and the surface mass balance from a regional atmospheric climate model in Greenland (RACMO2) (van Angelen et al., 2012), and discuss the connections between natural climate oscillations in the North Atlantic and the ice mass loss acceleration.

2. Greenland mass variations

Greenland's ice mass variations can be separated into those driven by surface mass balance (SMB) and ice discharge,

$$\Delta M_{T_0}^{T} = \int_{T_0}^{T} SMBdt - \int_{T_0}^{T} Ddt = \int_{T_0}^{T} (P-R)dt - \int_{T_0}^{T} Ddt \quad (1)$$

in which $\Delta M_{T_0}^{T}$ is ice mass change from T_0 to T, and P, R and D are precipitation, runoff and ice discharge, respectively. We ignore sublimation (Lenaerts et al., 2012) and basal melting of grounded ice here because they represent small mass loss terms and expected to be relatively constant over the periods analyzed here.

We independently estimate $\Delta M_{T_0}^{T}$ using the GRACE monthly gravity solutions (CSR RL05), consisting of spherical-harmonic (SH) coefficients of the Earth's gravitational potential, complete to degree and order up to 60, from January 2003 to December 2012. Degree 2 and order 0 SH coefficients are replaced by the satellite laser ranging (SLR) estimates (Cheng and Tapley, 2004) because the former include a larger alias error from ocean tides (Seo et al., 2008). The degree 1 coefficients associated with center of mass change of the Earth are not observable from GRACE, and thus we include these terms estimated by GRACE information combined with numerical models (Swenson et al., 2008). The Glacial Isostatic Adjustment (GIA) effect is corrected using the model of Paulson et al. (2007) in the SH domain. To suppress peculiar north–south stripes and noise in GRACE data, the correlated patterns in SH coefficients are removed from SH order 8 and higher (Swenson and Wahr, 2006) and a 300 km Gaussian filter is applied. Since Greenland is closely located to the Canadian Arctic Archipelago (CAA) in which sharp ice mass loss has occurred (Jacob et al., 2012), the ice mass loss in CAA likely contaminates gravity changes in Greenland as a leakage error. To account for the leakage error, we convert ice mass loss data in CAA (Gardner et al., 2011) to SH coefficients. The SH coefficients are smoothed by a 300 km Gaussian filter and subtracted from GRACE SH coefficients. The leakage effect in Greenland from the CAA is about −4.1 Gt/yr for the linear trend and −1.0 Gt/yr^2 for the acceleration.

Finally, we estimate latitude–longitude grid (1°× 1°) values for Greenland from the reduced SH coefficients based on the forward modeling method (Chen et al., 2013). We first generate random numbers in Greenland. The randomly distributed initial mass fields are smoothed by a 300 km Gaussian filter. Differences at each grid are computed from the smoothed initial fields and the smoothed fields estimated from the reduced SH coefficients, and they are added to the initial fields for update ice mass fields. The same procedure continues with the updated ice mass fields until the smoothed updated fields are close to the smoothed estimated field from the reduced SH coefficients within a defined threshold, 36.6 Gt, which is the GRACE random noise over Greenland. The random noise is quantified based on the root mean squared (RMS) of GrIS mass variations from the difference between SH coefficients and smoothed SH coefficients (Velicogna and Wahr, 2013).

Fig. 1(a) shows the integrated Greenland ice mass change, $\Delta M_{T_0}^{T}$ (blue), and SMB accumulation, $\int_{T_0}^{T} SMBdt = \int_{T_0}^{T} (P-R)dt$ (red), when T_0 is January 2003. To examine monthly SMB in Greenland, we use the RACMO2 monthly precipitation and runoff data. It clearly shows that Greenland ice mass has been decreasing since Jan. 2003 with a significant negative trend (−244.0 ± 28.2 Gt/yr). Table 1 shows linear trends from previous studies that were estimated by different data processing techniques: forward modeling in grid points (Chen et al., 2013) and sub-basins (Wouters et al., 2013), mascon (Luthcke et al., 2013), Slepian basis (Harig and Simons, 2012) and averaging kernel (Velicogna and Wahr, 2013). Numbers in parentheses are our results with 95% confidence interval during the same period of each previous study. In general, our estimates agree with those from previous studies within the uncertainty ranges. The uncertainties are estimated based on a Monte Carlo (MC) experiment. For the MC experiment, we first estimate uncertainties in random noise (36.6 Gt), removing the correlated patterns (12.3 Gt) and the misfit of the linear trend to $\Delta M_{T_0}^{T}$ (142.6 Gt). Because the de-correlation procedure in SH coefficients possibly removes real signals, we calculate the difference in GrIS mass changes between results obtained before and after applying the de-correlation and estimate RMS of the difference. Combining the three errors based on the root sum squared, the total monthly error is estimated to be 147.7 Gt. Finally, 1000 random numbers with normal distribution having a mean of 0 and a standard deviation of 147.7 Gt are generated for each month. For the linear trend uncertainty, we also add ICE-5G GIA model error in Greenland, 19 Gt/yr (Velicogna and Wahr, 2013).

The cumulative SMB for the decade is about 3509 Gt, and its seasonal cycle is in-phase with the Greenland ice mass variation. The difference between the ice mass change and the cumulative SMB represents the cumulative ice mass loss from ice discharge (Fig. 1b). The mean ice discharge from 2003 to 2012 is 587.5 ± 30.8 Gt/yr (95% confidence level), and this estimate is close to the ice discharge estimate based on ice-penetrating radar survey (Enderlin et al., 2014): their range is from 510 Gt/yr to 550 Gt/yr from 2003 to 2012. To examine the interannual variability in the total ice mass loss and the cumulative SMB, we remove linear trends and annual cycles from both time series, and these reduced time series are shown in Fig. 1(c). The reduced fields are denoted by ΔM_* and $SMB_*(=P_* - R_*)$. Both of the basin integrated ΔM_* and SMB_* exhibit very similar variations, increasing from 2003 to 2008 and decreasing afterwards, with a transient decrease during 2007 and 2008. Error bars are shown as the same color of the ΔM_* and SMB_*. The SMB uncertainty is estimated based on the RACMO2 model error, which is estimated to be about 18% of the model output (Ettema et al., 2009).

Both lines clearly show a similar quadratic pattern, implying that Greenland's ice mass loss acceleration is due mostly to SMB variations (Sasgen et al., 2012). The acceleration rate obtained here from 2003 to 2012 is −13.9 ± 2.0 Gt/yr^2 and close to the acceleration rate in SMB_*, −11.1 ± 1.2 Gt/yr^2. The acceleration rates are calculated from the 2nd order polynomial ($a_0 + a_1t + a_2t^2$) fitting to the basin integrated ΔM_* and SMB_*, and the uncertainties represent the 95% confidence level that is quantified with the analogous MC experiment. Similar to the linear trend, we estimate acceleration rates in different periods to compare them with previous studies (Table 1). Our estimates agree with those from previous studies within the uncertainty ranges, and are, in particular, very close to the forward modeling method in sub basins (Wouters et al., 2013) and the Slepian basis method (Harig and Simons, 2012).

Fig. 1(d) shows ice discharge ($-D_*$) and its uncertainty after removing a linear trend and seasonal cycle from the cumulative ice discharge shown in Fig. 1(b). Compared with SMB_*, its variation is minor implying that ice discharge variation is rather stable from 2003 to 2012 (Enderlin et al., 2014). However, it shows an apparent increase of ice discharge in 2012. It is not certain how to explain this, but the possible causes would be the change of ice dynamics and/or underestimate of SMB. We further

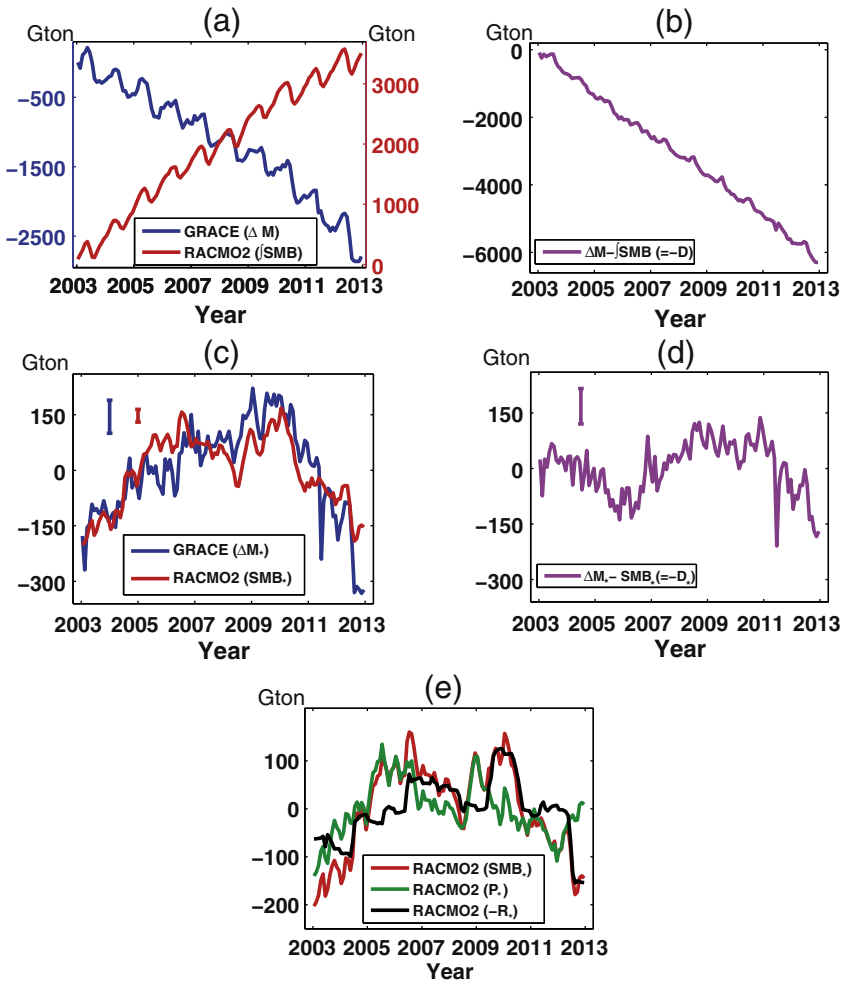

Fig. 1. (a) Greenland mass change observed by GRACE (blue) and cumulative SMB from RACMO2 (red). (b) Cumulative ice mass loss due to ice discharge in Greenland. (c) As in Fig. 1a except after removing linear trends and seasonal cycles. Both lines clearly show a similar quadratic pattern, implying that Greenland's mass loss acceleration is due to the SMB variation. (d) As in Fig. 1b except after removing a linear trend and seasonal cycle. (e) Greenland cumulative SMB's (red) contributions from precipitation (green) and runoff (black).

examine the contributions of precipitation and runoff to the Greenland SMB acceleration (Fig. 1(e)). From 2003 to 2009, the variation of SMB_* (red) is close to that of P_* (green). On the other hand, $-R_*$ (black) contributes significantly less to SMB_* variations from 2003 to 2008, however, its variation is much larger than precipitation since 2009. The pulse shaped SMB_* variation during 2009 and 2010 and the significant drop of SMB_* in 2012 are mostly explained by the runoff, and these patterns are consistent with the low value of surface melting in 2009 and record high melting in 2010 and 2012 (Tedesco et al., 2011, 2013; Nghiem et al., 2012). The ice mass loss acceleration rate in P_* and $-R_*$ from 2003 to 2009 is -9.7 ± 2.5 Gt/yr^2 and -2.1 ± 2.2 Gt/yr^2, respectively. However, the rate in $-R_*$ (-6.3 ± 1.1 Gt/yr^2) is larger than that in P_* (-4.8 ± 1.1 Gt/yr^2) when the time span is extended up to 2012. This is because the larger drop in $-R_*$ and increase in P_* during 2012. Consequently, those results imply that acceleration in Greenland ice mass loss is attributed to the precipitation decrease from 2003 to 2009 (van den Broeke et al., 2009; Sasgen et al., 2012) while the contribution from runoff is emerging as an important contribution in the summers of 2010 and 2012.

The spatial pattern of the acceleration rate in ΔM_* is shown in Fig. 2. Most acceleration of ice mass loss was occurred in the west coast. On the other hand, it shows minor acceleration of ice mass gain in the east coast. In general, regions of large acceleration are not located in ice sheet area but in tundra area. This is likely associated with GRACE's low spatial resolution and the inherent uncertainty in forward modeling, non-uniqueness. For example, GRACE observations of ice mass changes in the interior Greenland should spread out to the coasts and even to offshore area, and this is the cause of the leakage error. During the forward modeling, leakage error is estimated and added to the interior of Greenland, but larger ice mass is added to the coastal regions than to the interior regions because coastal areas are more vulnerable to the leakage. Therefore, local maxima and minima of ice mass anomalies are subject to be closer to the coasts as shown in the figure.

Because inter-annual variability in the Greenland ice mass change exhibits distinct spatial patterns (Chen et al., 2011), we examine the co-variations between GRACE (ΔM_*) and RACMO2 ($SMB_* = P_* - R_*$) in five Greenland basins (Zwally et al., 2012): north, west, east, south-west and south-east Greenland (Fig. 3a). Fig. 3b–f shows ΔM_* and SMB_* in these five different basins. In general, ΔM_* and SMB_* show similar variations within each basin, implying again that inter-annual variability in ice mass loss are caused mainly by SMB_* variations. However, different variability in each basin is also evident. In the north, both ΔM_* and SMB_* increase in 2007 and decrease afterward. In the west basin, they steeply increase until 2004 and gradually decrease afterward. Combined with a negative linear trend that is removed in our analysis, this pattern shows a relatively small ice mass loss from 2003 to 2004 and large losses after 2005, and agree with the previous finding concerning the acceleration of GrIS mass loss (Chen et al., 2011). In the east basin, the inter-annual variability is correlated but with a smaller amplitude than in the other basins. The ΔM_* and SMB_* time series in

Table 1
Linear trends and acceleration rates from different methods to account for leakage effect. Those methods include forward modeling in grid points (Chen et al., 2013), forward modeling in sub-basins (Wouters et al., 2013), MASCON (Luthcke et al., 2013), Slepian basis (Harig and Simons, 2012) and averaging kernel (Velicogna and Wahr, 2013). Linear trends and acceleration rates from this study are shown in parentheses during the same periods of the previous studies. To compare with Harig and Simons (2012), we use GRACE data from Jan. 2003 to Aug. 2011 because RL05 is available only after 2003. Since Wouters et al. (2013) and Velicogna and Wahr (2013) estimated the acceleration rate from the 2nd order polynomial coefficients scaled by a factor of 1/2 ($a_0 + a_1 t + a_2/2\ t^2$), their acceleration rates are scaled down by 1/2 to be comparable with other estimates. Trend and acceleration units are Gt/yr and Gt/yr^2, respectively.

	Trend	Acceleration
Chen et al. (2013) from 01/2005 to 12/2011	−252.2 ± 18.3 (−239.4 ± 31.3)	N/A
Wouters et al. (2013) from 01/2003 to 09/2012	−249.0 ± 20.0 (−239.9 ± 18.2)	−12.5 ± 9.0 (−12.8 ± 2.1)
Luthcke et al. (2013) from 12/2003 to12/2010	−230.3 ± 12.1 (−210.4 ± 29.3)	−10.1 ± 6.3 (−6.2 ± 3.8)
Harig and Simons (2012) from 04/2002 to 08/2011	−199.7 ± 6.3 (−220.2 ± 18.1)	−8.7 ± 4.1 (−8.9 ± 2.7)
Velicogna and Wahr (2013) from 01/2003 to 11/2012	−258.0 ± 41.0 (−242.8 ± 18.3)	−15.6 ± 6.0 (−13.6 ± 2.0)

south-west exhibits increase in two different periods during 2003/05 and 2008/09, and a decrease during 2006/07 and 2010/11. In the south-east, both time series increase during 2003 and 2008/2009 while they decrease during other periods. This result is consistent with a previous finding (Chen et al., 2011) that south-east Greenland has experienced relatively small ice mass loss during 2002/04 and 2008/09 and a larger ice mass loss between these two periods. Therefore, these findings show that SMB dominates the inter-annual ice mass changes of the GrIS in each basin of Greenland and is consistent with Fig. 1c for the entire ice sheet. However, relatively larger differences between ΔM_* and SMB_* are observed in the south-west basin from 2003 to 2006 and in the south-east basin from 2007 to 2012. It is not obvious how to explain the misfit between observation and model in this case. Ice discharge variation is a likely cause to explain the misfit. Another suggestion is that the south-east and south-west basins are in close proximity, and thus GRACE observations with their lower spatial resolution might not be able to cleanly distinguish gravity changes from the two regions. To examine this, we smooth SMB_* with a 300 km Gaussian filter similar to GRACE and apply the forward modeling for the smoothed SMB_* fields. Fig. S1 shows true SMB_* (red) and estimated SMB_* (blue) from forward modeling with the smoothed SMB_*. The two time series are very close in the north, east and west basins. However, in south-west and south-east, they show similar differences exhibited in Fig. 2 while the sum of both basins for true and estimated SMB_* exhibit very similar variations. Therefore, the misfit in the south-east and south-west basin is partly associated with uncorrected leakage effect between the two basins. Table 2 summarizes acceleration rates for the five basins.

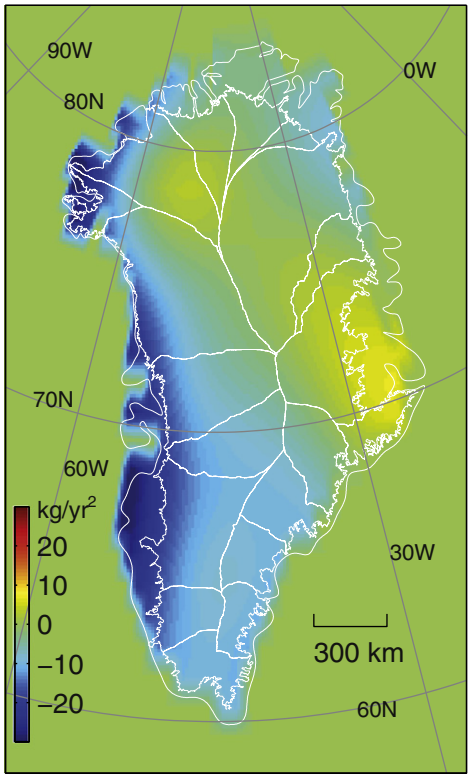

Fig. 2. Spatial pattern of acceleration rate in mass change (ΔM_*). Unit is kg/yr^2.

Similar to Fig. 1(e), we separate SMB_* into precipitation (P_*) and runoff ($-R_*$) for the five separate basins and show these in Fig. 4. In the north basin, the larger SMB_* change in 2006 and 2007 is almost equally explained by $-R_*$ and P_*. In other four basins, P_* appears to be the main cause to explain the SMB_* variation from 2003 to 2009, but $-R_*$ is significant after 2010. Significant SMB_* and $-R_*$ drop in 2012 is evident in all five basins, particularly in south-west. This result again indicates that runoff is important for the GrIS mass loss acceleration in the most recent years, and P_* was the main cause for the GrIS mass loss acceleration before 2010, in all five of the basins (Sasgen et al., 2012). Acceleration rates and their uncertainties during periods of 2003–2009 and 2003–2012 in the five basins are summarized in Table 3.

Based on the results discussed above, the Greenland ice mass loss acceleration from 2003 to 2012 can be attributed to both precipitation decrease and runoff increase. From 2003 to 2009 the decrease in precipitation appears to be the dominant cause to explain the ice mass loss acceleration of the GrIS, and the melt water runoff is more important to the acceleration after this period due to the extreme melting in 2010 and 2012. To examine the co-variability of the ΔM_* and P_* (and $-R_*$) in more detail to understand the time history of ice mass loss and examine whether it exhibits the above characteristics, we apply combined EOF (CEOF) analysis (Kutzbach, 1967) for the gridded ΔM_* and P_*. The principal components (PCs) are normalized to have unit variance and consequently the CEOF patterns are normalized to the variance explained by the given mode and thus have units of mm of water. The PC time series from the 1st CEOF mode (Fig. 5a) from ΔM_* and P_* shows very similar temporal variations to those shown in Fig. 1, increasing until 2006 and decreasing afterwards. The co-variance explained by the 1st CEOF is 43%, and the variances of ΔM_* and P_* explained are 36% and 50%, respectively. The 1st CEOF mode for ΔM_* (Fig. 5b) exhibits a dipole pattern, positive in the west and negative in the east. Fig. 5c is the corresponding 1st mode CEOF of P_*, which also shows a similar dipole pattern to Fig. 5b. However the two modes (Fig. 5b and c) show two different spatial characteristics: the positive anomaly in ΔM_* extends from south-west to north-west, and the negative anomaly in south-east that is evident in P_* is not evident in ΔM_*. As discussed above, the ΔM_* is an integrated observation including precipitation, runoff and ice discharge. Therefore, the apparent acceleration

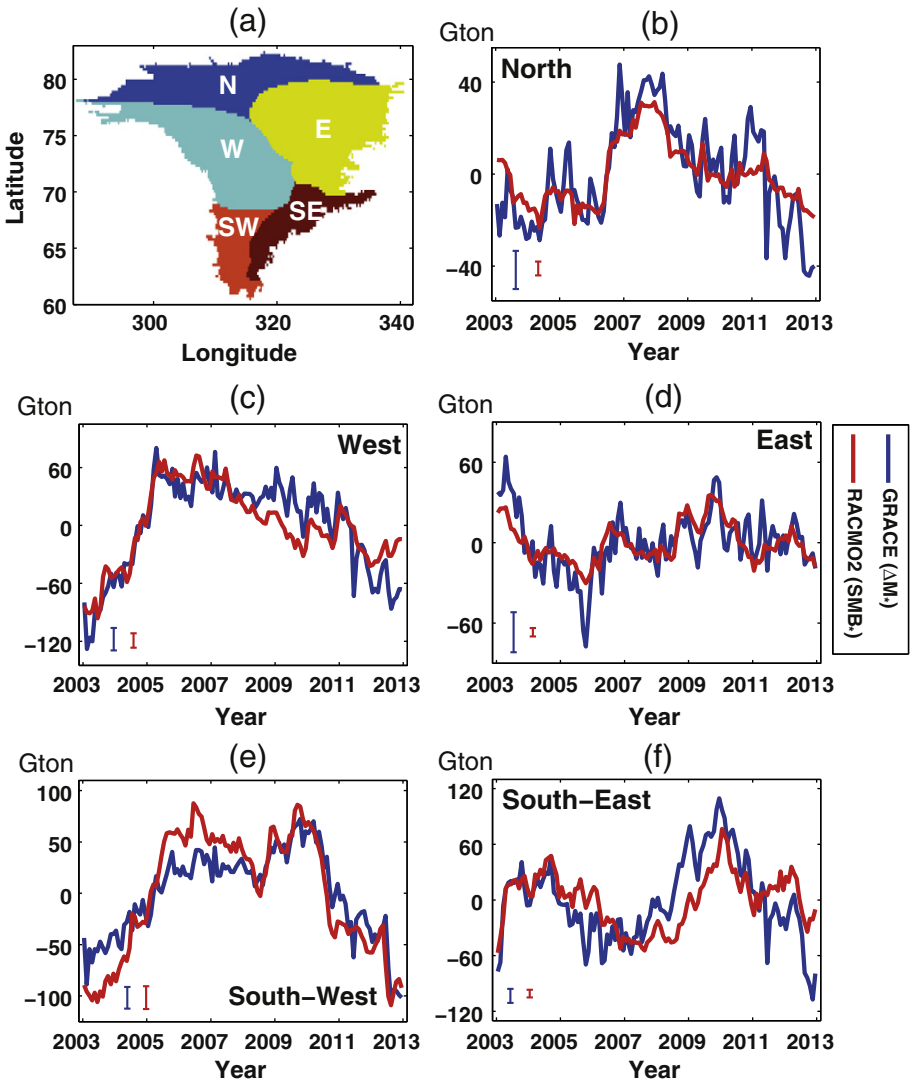

Fig. 3. Five main basins in Greenland (a) and mass change (ΔM_*) and cumulative SMB_* in the basins (b–f). Linear trends and seasonal cycles are removed. In all basins, ΔM_* and SMB_* show similar accelerated patterns.

anomaly in the north-west and west that is shown in the first CEOF mode of ΔM_* appears to be partly associated with increasing runoff and/or ice discharge. Similarly, ΔM_* in the south-east may include both effects from both an increase in runoff and in precipitation, and thus the mass increase from the precipitation increase (negative anomaly in the CEOF mode of P_* in south-east) is likely diminished by the mass decrease from runoff increase. Therefore, the negative anomaly in south-east exhibited in the CEOF mode of P_* may not be expected to be exhibited in ΔM_*.

Similar to Fig. 5, Fig. 6 shows the CEOF of ΔM_* and $-R_*$. The covariance of the 1st CEOF is 56%, accounting for 49% and 62% of ΔM_* and $-R_*$ variance, respectively. The first PC time series shows the apparent variation of anomalously large runoff in 2010 and 2012. The 1st CEOF modes from ΔM_* and $-R_*$ exhibit strong positive anomalies from south-west to north-west Greenland and weak positive anomaly in south-east. In general, regions of positive anomalies in CEOF mode of ΔM_* agree with those of $-R_*$, but their exact locations differ, which is likely due to GRACE's low spatial resolution and the nature of non-uniqueness for forward modeling as discussed in Fig. 2. As discussed above, the locations of these positive anomalies agree with regions where the CEOF mode of ΔM_* in Fig. 5 is not consistent with that of P_*. As a result, the discrepancies between the two CEOF modes in Fig. 5 result from the contribution and pattern from meltwater runoff. The CEOFs from Figs. 5 and 6 show that the ice mass loss acceleration in Greenland is mostly along the west coast due to a decrease in precipitation and an increase in meltwater runoff.

Table 2
Acceleration rates with 95% confidence interval in sub-basins observed by GRACE.

Sub-basins	Acceleration rate
N	-2.0 ± 0.4
E	0.2 ± 0.6
W	-5.0 ± 0.5
SE	-2.1 ± 0.9
SW	-5.0 ± 0.5
Total	-13.9 ± 2.9

3. Large scale circulation oscillations in the North Atlantic and precipitation in Greenland

In the previous section, we show that the acceleration of GrIS mass loss over the last decade is primarily affected by variability in both precipitation and meltwater runoff. The increase of meltwater runoff has been shown to be related to the increase occurrences of the negative phases of the North Atlantic Oscillation (NAO) during summer, which

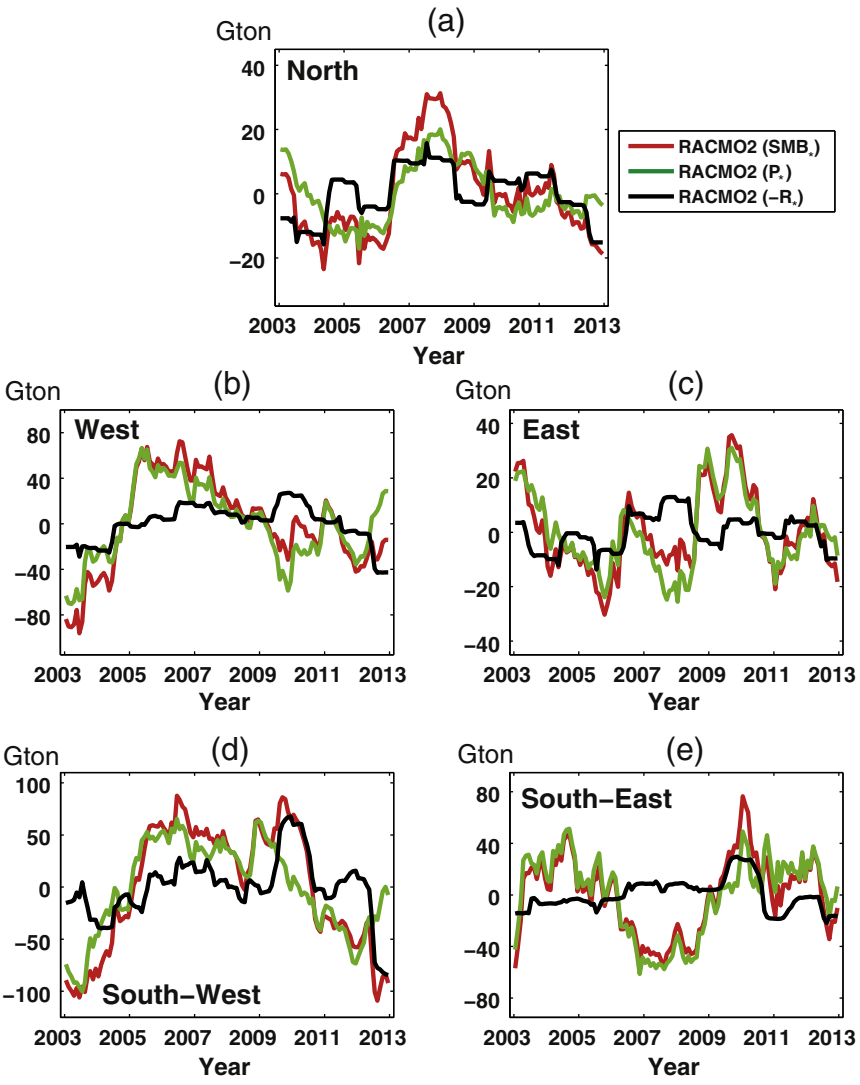

Fig. 4. Cumulative precipitation, P_* (green), runoff, $-R_*$ (black) and surface mass balance, SMB_* (red) after removing linear trends and seasonal cycles. In all five basins, P_* is very close to the SMB_* while $-R_*$ is significant in 2010 and 2012.

favors an anticyclonic circulation at upper levels and warmer conditions over Greenland at lower levels through the advection of warm air along its western coast (Fettweis et al., 2013). However, the connection between the NAO and the recent precipitation decrease has not yet been examined although it was reported that Greenland precipitation is negatively correlated with the NAO during winter (e.g., Hurrel, 1995). Therefore, the recent decrease of precipitation is possibly connected to NAO variations similar to meltwater runoff, so here we examine how the NAO influences Greenland precipitation. We first check the seasonal correlation between the NAO index and Greenland precipitation for each season from 1960 to 2012: spring (March–May), summer (June–August), fall (September–November) and winter (December–February) (Fig. 7a–d). The monthly NAO index is provided by the Climate Prediction Center, NOAA (Camp Springs, Maryland, http://www.cpc.ncep.noaa.gov), and their seasonal variations are shown in Fig. S2. To test the correlation between NAO and P and examine its temporal evolution to check if the recent precipitation decrease is unusual or not, we calculate the correlation coefficients centered on each year using a sliding 7-year window (Fig. 7). For example, the coefficient during summer 2000 is calculated with NAO and P from 1997 to 2003. The dotted lines in Fig. 7 exhibit 95% confidence level of the correlation. The temporal variations of the correlation show that spring and fall

Table 3
Acceleration rates with 95% confidence interval in SMB_*, P_* and $-R_*$ for five basins. Unit is Gt/yr^2.

	2003–2009			2003–2012		
	SMB_*	P_*	$-R_*$	SMB_*	P_*	$-R_*$
N	-0.5 ± 0.8	0.5 ± 0.6	-1.0 ± 0.4	-1.0 ± 0.3	-0.3 ± 0.2	-0.8 ± 0.1
E	3.1 ± 0.6	3.4 ± 0.6	-0.2 ± 0.4	-0.1 ± 0.4	0.3 ± 0.3	-0.4 ± 0.1
W	-10.5 ± 1.0	-9.2 ± 0.9	-1.3 ± 0.5	-4.0 ± 0.6	-2.1 ± 0.7	-1.9 ± 0.2
SE	3.4 ± 1.6	3.1 ± 1.6	0.2 ± 0.3	1.2 ± 0.7	2.2 ± 0.7	-1.0 ± 0.2
SW	-7.3 ± 1.6	-7.5 ± 1.1	0.2 ± 1.1	-7.2 ± 0.6	-4.9 ± 0.6	-2.3 ± 0.6
Total	-11.8 ± 3.1	-9.7 ± 2.5	-2.1 ± 2.0	-11.1 ± 1.2	-4.8 ± 1.1	-6.3 ± 1.0

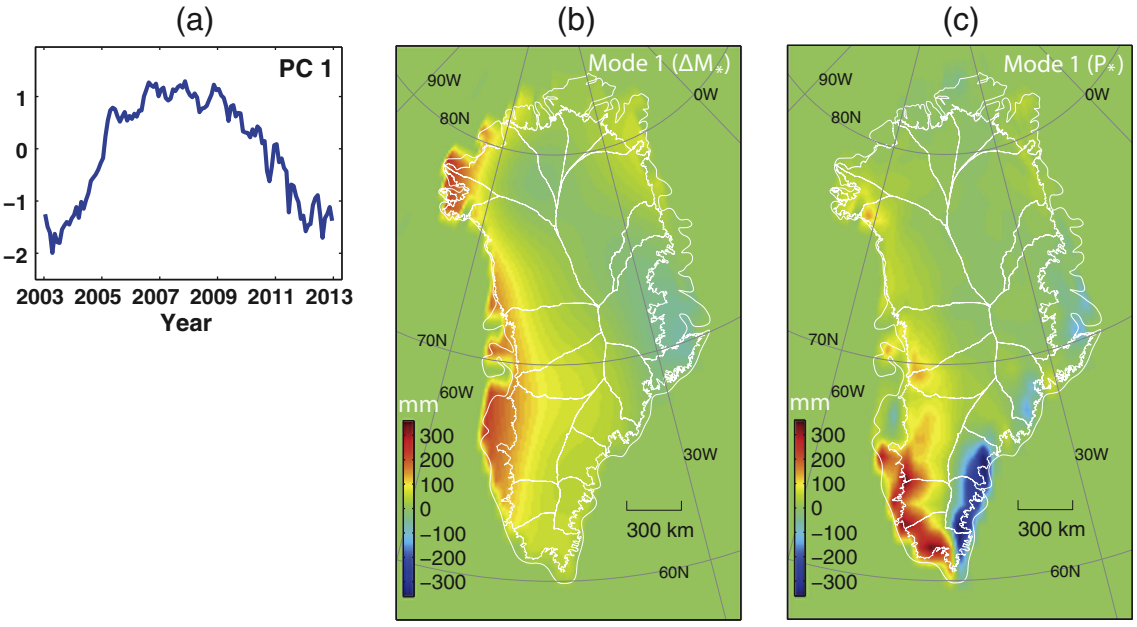

Fig. 5. (a) The principal component (PC) of the leading mode from the combined EOF with the data field associated with gridded ΔM_* and P_* after removing linear trends and seasonal cycles. (b) The first modes of the combined EOFs with data field associated with gridded ΔM_* and P_*. It is the portion of the combined EOF associated with Greenland's mass change (GRACE). (c) is analogous to (a), except for cumulative precipitation (RACMO2).

precipitation are not consistently correlated with the NAO. However, it is evident that the summer (winter) precipitation exhibits a rather consistent positive (negative) correlation with the NAO. It is interesting to note that the correlation pattern was opposite to the norm (or at least weak) in the late 1990s and then returns to more typical values in about 2006. In addition, there was an apparent positive correlation for winter during late 1960s to early 1970s.

The correlation pattern changes in the late 1990s possibly results from NAO pattern changes. Zhang et al. (2008) found that the poleward center of the NAO shifted from the Icelandic Sea to the Eurasian Arctic coast since 1986, and this progressive eastward shift was abrupt since the beginning of the 21st century. The change in the NAO spatial pattern might systematically influence the nature of the storm tracks and the precipitation pattern in the North Atlantic. Therefore, it is important to examine further if the recent NAO pattern change is connected to the recent precipitation decrease in GrIS. To examine this, the seasonal mean NAO index is regressed on seasonal mean precipitation fields during winter and summer. We examine the regression maps in five different

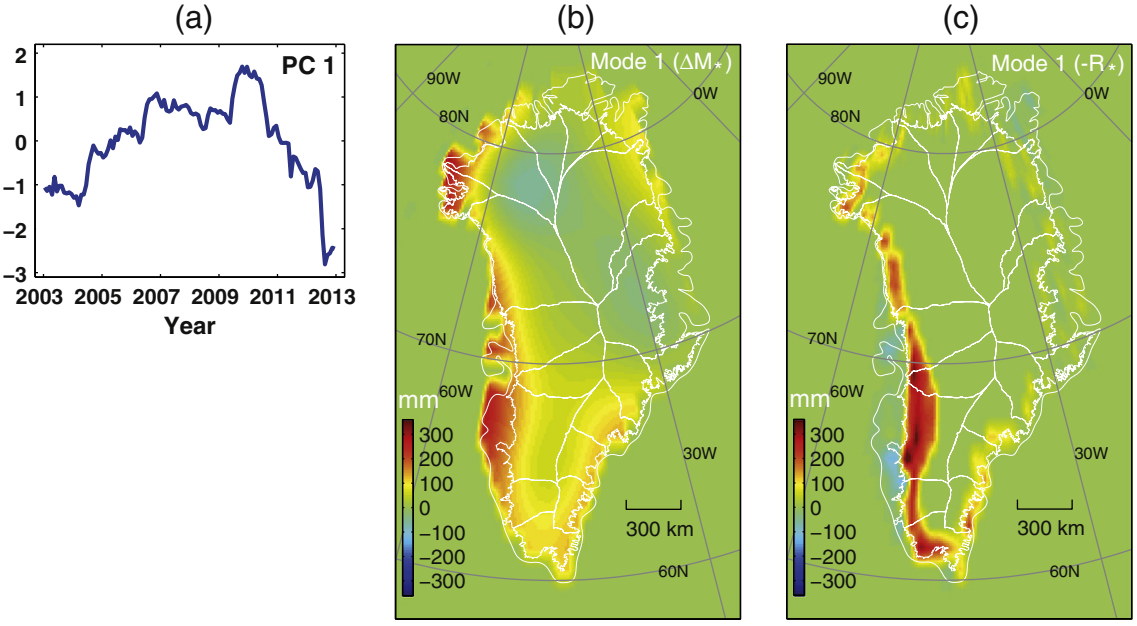

Fig. 6. (a) The principal component (PC) of the leading mode from the combined EOF with the data field associated with gridded ΔM_* and $-R_*$ after removing linear trends and seasonal cycles. (b) The first modes of the combined EOFs with data field associated with gridded ΔM_* and $-R_*$. It is the portion of the combined EOF associated with Greenland's mass change (GRACE). (c) is analogous to (a), except for cumulative meltwater runoff (RACMO2).

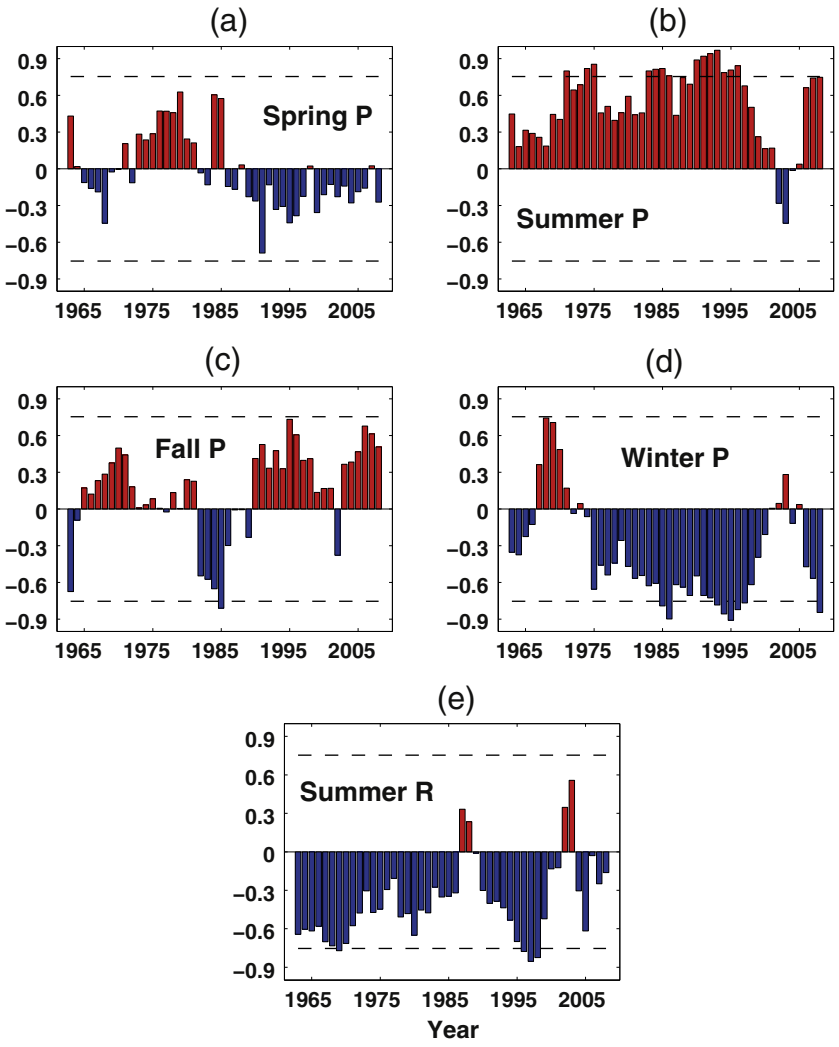

Fig. 7. Correlation coefficients between NAO and P (a–d) and NAO and R (e).

decadal periods, 1967–1976, 1977–1986, 1987–1996, 1997–2006 and 2003–2012. We select periods of 1997–2006 and 2003–2012 separately to examine the correlation pattern change shown in Fig. 7 and the precipitation accumulation pattern for GRACE period, respectively.

Before the regression, NAO index for the given period is normalized by its standard deviation after removing the mean, and the unit of precipitation is converted to kg. Fig. 8 shows the regression maps during winter. As suggested by Fig. 7d, the winter regression pattern during 1967–1976 differs most from other periods: dominant positive anomalies are located in south-east Greenland while other regression maps show negative anomalies. The patterns during 1977–1986 and 1987–1996 are rather similar to each other showing large negative anomalies in south-east while there are minor positive anomalies in south-west during 1977–1986. The regression map during the period of 1997–

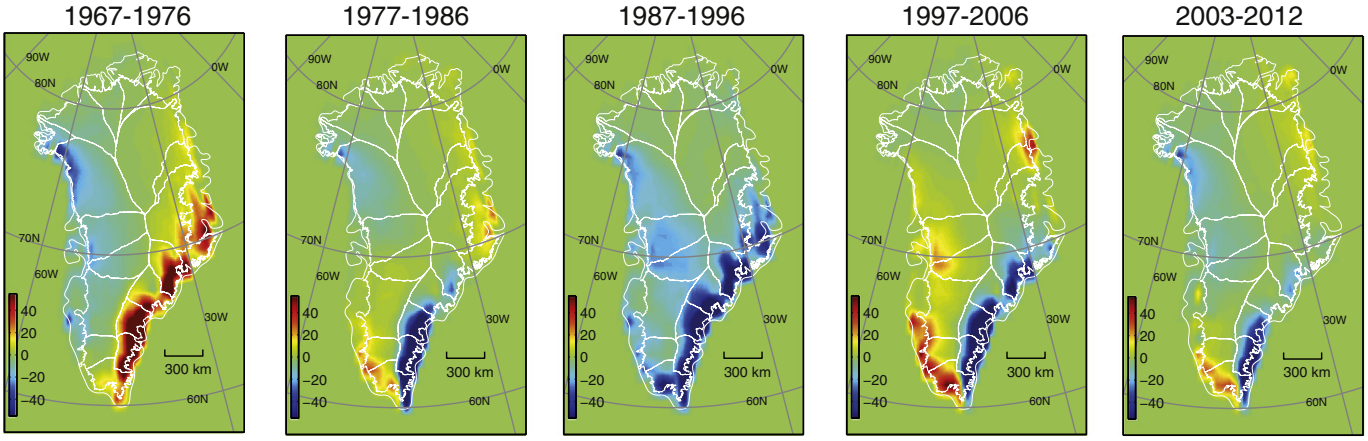

Fig. 8. Regression maps of NAO on precipitation fields during winter.

Table 4
Seasonal acceleration rates with 95% confidence interval in P_* and $-R_*$. Unit is Gt/yr^2.

	1967–1976	1977–1986	1987–1996	1997–2006	2003–2012
Winter P_*	-0.6 ± 3.2	-1.0 ± 1.9	1.4 ± 3.3	1.7 ± 1.1	1.0 ± 1.3
Summer P_*	5.2 ± 1.7	2.9 ± 2.1	0.7 ± 1.1	0.9 ± 1.0	-3.7 ± 1.2
Summer $-R_*$	2.8 ± 3.0	-0.3 ± 2.0	0.3 ± 2.7	-5.1 ± 2.8	-7.8 ± 3.4

2006 exhibits distinct spatial characteristic that exhibit strong dipole patterns; positive anomalies in south-west and negative anomalies in south-east. The regression map during the GRACE period shows a similar dipole pattern, more closely resembling the pattern during 1977–1986. In addition, this is close to the CEOF mode of P_* in Fig. 5c although the positive anomalies in south-west are smaller than those in Fig. 5c compared to the negative anomalies in the south-east. We also examine acceleration rates of the anomalous precipitation accumulation (P_*) during the five different periods in Table 4. Any significant ice mass loss acceleration associated with precipitation decrease has not occurred. As a result, we conclude that the winter NAO plays an important role in Greenland precipitation during GRACE period, but it would not be a cause to explain the contemporary ice mass loss acceleration in GrIS.

Summer regression maps exhibit similar precipitation pattern changes (Fig. 9) although different than the winter maps. In general, positive anomalies are significant in the south-west during the periods of 1967–1976 and 1977–1986. However, locations of the positive anomalies were shifted to south-east during 1997–2006, and this pattern remains during GRACE period. Table 4 summarizes the acceleration rates from summer precipitation accumulation (P_*) during the five periods. Significant ice mass loss acceleration is only observed during the GRACE period. On the other hand, the summer regression map during GRACE period does not agree with the CEOF mode of P_* in Fig. 5c while the winter map does show a similar dipole pattern. Because Fig. 5c includes precipitation anomalies from both winter and summer seasons, we add the winter and summer regressions maps (Fig. 10) to be more comparable with the CEOF mode of Fig. 5c. It is interesting to note that, for GRACE period, the combined winter and summer regression maps closely resemble the CEOF mode in Fig. 5c. Therefore, the current anomalous GrIS precipitation accumulation, which can partly account for the ice mass loss acceleration, is mostly associated with winter and summer NAO and possibly its pattern change.

We apply the same regression analysis for the ice mass change associated with the anomalous accumulation of the meltwater runoff ($-R_*$). Correlation coefficients between meltwater runoff and NAO also show similar pattern changes (Fig. 7e), and thus we use the same examination periods, 1967–1976, 1977–1986, 1987–1996, 1997–2006 and 2003–2012. Fig. 11 shows that there are strong positive anomalies

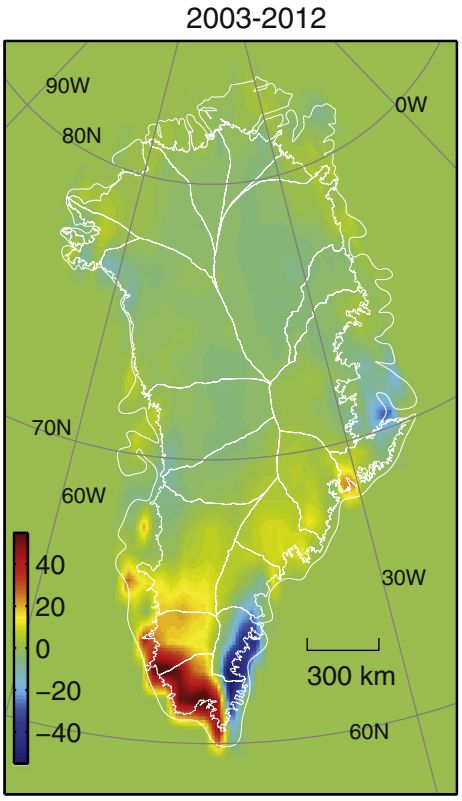

Fig. 10. Combined regression map of NAO and precipitation fields during winter and summer from 2003 to 2012.

in the west during the periods of 1967–1976 and 1977–1986, and the anomalies are suppressed during 1987–1996. Similar to winter and summer precipitation, the regression map during 1997–2006 exhibits a different spatial pattern: positive anomalies occur in the south-west and negative anomalies are found in the west and east. During GRACE period, there are strong positive anomalies from south-west to north-west of Greenland. The acceleration rates are also presented in Table 4. Before the NAO pattern change in the late 1990s, the increase of meltwater runoff is not apparent, but a significant increase of meltwater runoff started during 1997–2006 and continues until 2012. In particular, the regression pattern during GRACE period is remarkably similar to that of the CEOF mode of $-R_*$ in Fig. 6c. As a result, the meltwater runoff in Greenland is also influenced by the NAO (Fettweis et al., 2013).

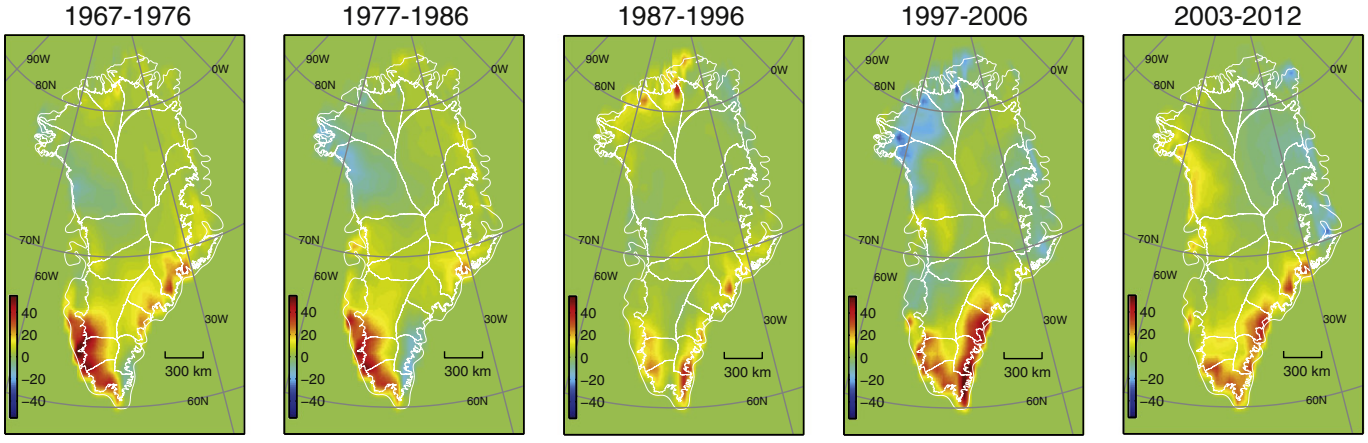

Fig. 9. Regression maps of NAO on precipitation fields during summer.

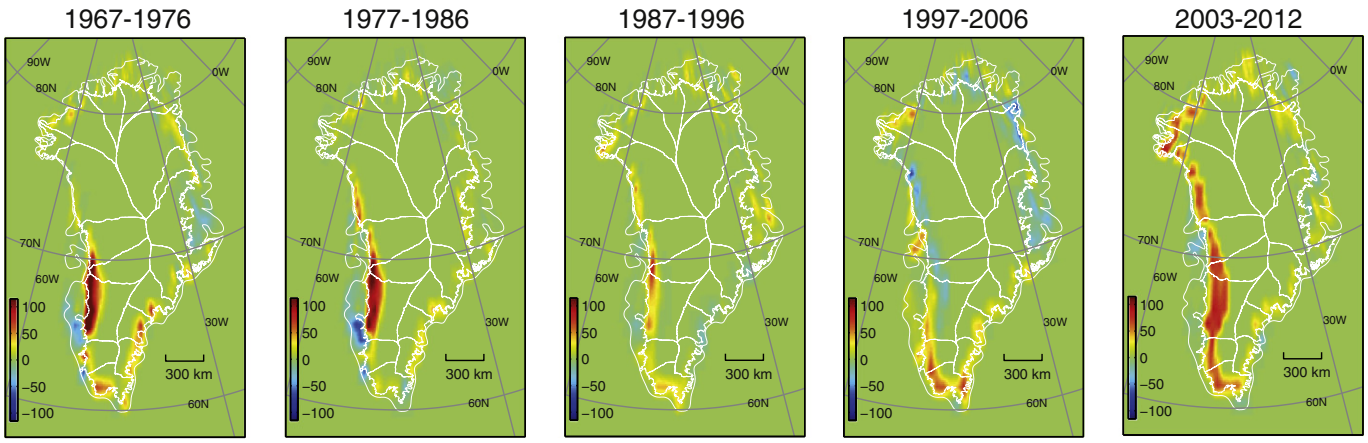

Fig. 11. Regression maps of NAO on meltwater runoff fields during summer.

4. Discussions and conclusions

Satellite remote sensing observations suggest an acceleration of Greenland's ice mass loss. The acceleration may be explained by an increase of mass loss from runoff and ice discharge or a decrease of mass gain from precipitation or a combination of both. Previously, the acceleration in ice mass loss was suggested to stem from both increasing runoff and discharge from 1958 to 2010 based on RACMO2 SMB data while in the most recent period (2003–2010) decreasing precipitation was found to be more significant to the acceleration (van den Broeke et al., 2009; Sasgen et al., 2012). Based on GRACE mass change and RACMO2 SMB data, we show that the acceleration rate from the decrease of precipitation is -9.7 ± 2.5 Gt/yr^2 and that from the increase of runoff is -2.1 ± 2.2 Gt/yr^2 from 2003 to 2009, which confirms the previous finding that the decrease of precipitation is the larger contributor than the increase of meltwater runoff and discharge for this period. We also find that the acceleration rate of GrIS mass loss from 2003 to 2012 is -13.9 ± 2.0 Gt/yr^2, and the decrease in SMB alone produces a similar acceleration rate, -11.1 ± 1.2 Gt/yr^2, implying that ice discharge is not significant in the recent acceleration (Enderlin et al., 2014). The increase of meltwater runoff (-6.3 ± 1.1 Gt/yr^2), resulting from the recent extreme melting in 2010 and 2012, contributes to the recent acceleration more than the decrease of precipitation (-4.8 ± 1.1 Gt/yr^2).

Accelerations associated with precipitation and meltwater runoff are only significant during summer, indicating the important role of summer in Greenland ice mass loss. It has been reported that the recent increase of meltwater runoff is due to the increase of negative phase of NAO during summer (Fettweis et al., 2013). In this study, we also find that NAO affects the decrease of summer precipitation. The NAO pattern change (Zhang et al., 2008) that occurred since 1986 might be one of the causes because regression maps before and after 1986 show distinct spatial patterns. Therefore, the findings in our study suggest that the negative NAO phases occurring recently in summer (Fettweis et al., 2013) and the pattern changes are important to GrIS mass loss acceleration. Because a major part of acceleration in GrIS mass loss is associated with precipitation decrease and runoff increase driven by the NAO, and the connection between precipitation and NAO in Greenland is suggested to undergo changes, caution must be exercised in inferring future sea level rise from the recent decade of satellite observations (Wouters et al., 2013).

Supplementary data to this article can be found online at http://dx.doi.org/10.1016/j.gloplacha.2015.02.006.

Acknowledgments

This work was supported by National Research Foundation grant NRF-2013R1A1A2008368 and Korea Polar Research Institute (KOPRI) research grant PM14020. DW and BT's contribution was carried out on behalf of the Jet Propulsion Laboratory, California Institute of Technology, under a contract with NASA. MRvdB and JHvA acknowledge support from the Netherlands Polar Program of the Netherlands Organization for Scientific Research (NWO/ALW).

References

Appenzeller, C., Schwander, J., Sommer, S., Stocker, T.F., 1998. The North Atlantic Oscillation and its imprint on precipitation and ice accumulation in Greenland. Geophys. Res. Lett. 25 (11), 1939–1942.
Box, J.E., 2006. Greenland ice sheet surface mass-balance variability: 1991–2003. Ann. Glaciol. 42 (1), 90–95.
Chen, J.L., Wilson, C.R., Tapley, B.D., 2011. Interannual variability of Greenland ice losses from satellite gravimetry. J. Geophys. Res. 116 (B07406).
Chen, J.L., Wilson, C.R., Tapley, B.D., 2013. Contribution of ice sheet and mountain glacier melt to recent sea level rise. Nat. Geosci. 6, 549–552.
Cheng, M., Tapley, B.D., 2004. Variations in the Earth's oblateness during the past 28 years. J. Geophys. Res. 109, B09402.
Dowdeswell, J.A., 2006. The Greenland ice sheet and global sea-level rise. Science 311, 963–964.
Enderlin, E.M., et al., 2014. An improved mass budget for the Greenland ice sheet. Geophys. Res. Lett. 41.
Ettema, J., van den Broeke, M., van Meijgaard, E., van de Berg, W., Bamber, J., Box, J., Bales, R., 2009. Higher surface mass balance of the Greenland ice sheet revealed by high-resolution climate modeling. Geophys. Res. Lett. 36 (L12501).
Fettweis, X., et al., 2013. Important role of the mid-tropospheric circulation in the recent surface melt increase over the Greenland ice sheet. Cryosphere 7 (241–248).
Gardner, A.S., et al., 2011. Sharply increased mass loss from glaciers and ice caps in the Canadian Arctic Archipelago. Nature 473, 357–360.
Harig, C., Simons, F.J., 2012. Mapping Greenland's mass loss in space and time. PNAS 109 (49), 19934–19937.
Hurrell, J., 1995. Decadal trends in the North Atlantic Oscillation: Regional temperatures and precipitation 269 (5224), 676–679.
Jacob, T., Wahr, J., Pfeffer, W.T., Sweson, S., 2012. Recent contributions of glaciers and ice caps to sea level rise. Nature 482, 514–518.
Johannessen, O.M., Khvorostovsky, K., Miles, M.W., Bobylev, L.P., 2005. Recent ice-sheet growth in the interior of Greenland. Science 310, 1013–1016.
Kutzbach, J.E., 1967. Empirical eigenvectors of sea-level pressure, surface temperature and precipitation complexes over North America. J. Appl. Meteorol. 6 (5), 791–802.
Lenaerts, J.T.M., van den Broeke, M.R., van Angelen, J.H., van Meijgaard, E., Dery, S.J., 2012. Drifting snow climate of the Greenland ice sheet: a study with a regional climate model. Cryosphere 6, 891–899.
Luthcke, S.B., et al., 2006. Recent Greenland ice mass loss by drainage system from satellite gravity observations. Science 314, 1286–1289.
Luthcke, S.B., Sabaka, T.J., Loomis, B.D., Arendt, A.A., McCarthy, Camp, J., 2013. Antarctica, Greenland and Gulf of Alaska land-ice evolution from an iterated GRACE global mascon solution. J. Glaciol. 59 (216), 613–631.
Mosley-Thompson, E., Readinger, C.R., Craigmile, P., Thompson, L.G., Calder, C.A., 2005. Regional sensitivity of Greenland precipitation to ANO variability. Geophys. Res. Lett. 32, L24707.
Nghiem, S.V., et al., 2012. The extreme melt across the Greenland ice sheet in 2012. Geophys. Res. Lett. 39 (L20502).
Paulson, A., Zhong, S., Wahr, J., 2007. Inference of mantle viscosity from GRACE and relative sea level data. Geophys. J. Int. 171, 497–508.
Pritchard, H.D., Arthern, R.J., Vaughan, D.G., Edwards, L.A., 2009. Extensive dynamic thinning on the margins of the Greenland and Antarctic ice sheets. Nature 461, 971–975.
Rignot, E., Kanagaratnam, P., 2006. Changes in the velocity structure of the Greenland ice sheet. Science 311 (17), 986–990.

Rignot, E., Velicogna, I., van den Broeke, M., Monaghan, A., Lenaerts, J.T.M., 2011. Acceleration of the contribution of the Greenland and Antarctic ice sheets to sea level rise. Geophys. Res. Lett. 38 (L05503).
Sasgen, I., et al., 2012. Timing and origin of recent regional ice-mass loss in Greenland. EPSL 333–334, 293–303.
Seo, K.-W., Wilson, C.R., Chen, J., Waliser, D.E., 2008. GRACE's Spatial Aliasing Error. 172, 41–48.
Shepherd, A., et al., 2012. A reconciled estimate of ice-sheet mass balance. Science 338 (30), 1183–1189.
Swenson, S., Wahr, J., 2006. Post-processing removal of correlated errors in GRACE data. Geophys. Res. Lett. 33, L08402.
Swenson, S., Chambers, D., Wahr, J., 2008. Estimating geocenter variations from a combination of GRACE and ocean model output. J. Geophys. Res. 113 (B08410).
Tedesco, M., et al., 2011. The role of albedo and accumulation in the 2010 melting record in Greenland. Environ. Res. Lett. 6.
Tedesco, M., Fettweis, X., Mote, T., Wahr, J., Alexander, P., Box, J., Wouters, B., 2013. The Cryosphere 7 (615), 630.
van Angelen, J.H., et al., 2012. Sensitivity of Greenland ice sheet surface mass balance to surface albedo parameterization: a study with a regional climate model. Cryosphere 6 (5), 1175–1186.
van den Broeke, M., et al., 2009. Partitioning recent Greenland mass loss. Science 326, 984–986.
Velicogna, I., 2009. Increasing rates of ice mass loss from the Greenland and Antarctica ice sheets revealed by GRACE. Geophys. Res. Lett. 36 (L19503).
Velicogna, I., Wahr, J., 2013. Time-variable gravity observations of ice sheet mass balance: precision and limitations of the GRACE satellite data. Geophys. Res. Lett. 40, 3055–3063.
Wouters, B., Bamber, J., van den Broeke, M.R., Lenaerts, J.T.M., Sasgen, I., 2013. Limits in detecting acceleration of ice sheet mass loss due to climate variability. Nat. Geosci. 6, 613–616.
Zhang, X., Sorteberg, A., Zhang, J., Gerdes, R., Comiso, J., 2008. Recent radical shifts of atmospheric circulations and rapid changes in Arctic climate system. Geophys. Res. Lett. 35 (L22701).
Zwally, H.J., Giovinetto, M.B., Beckley, M.A., Saba, J., 2012. Antarctic and Greenland Drainage Systems. GSFC Cryospheric Sciences Laboratory.